Thermogravimetric analysis and combustion efficiency analysis of *Jatropha carcus* biodiesel and its derivatives

Vinay Atgur [1,2,*], G. Manavendra[2], G. P. Desai[3], B. Nageswara Rao[1], I. M. Rizwanul Fattah[4,5*], Badr A. Mohamed[6,7], Nazaruddin Sinaga[8], H.H. Masjuki[9]

[1] *Department of Mechanical Engineering, Koneru Lakshmaiah Education Foundation (KLEF), Green Fields, Vaddeswaram, Guntur-522502, Andhra Pradesh, India*

[2] *Department of Mechanical Engineering, Bapuji Institute of Engineering and Technology (BIET), Davangere-577055, Karnataka, India*

[3] *Department of Chemical Engineering, Bapuji Institute of Engineering and Technology (BIET), Davangere-577055, Karnataka, India*

[4] *Centre for Green Technology, Faculty of Engineering and IT, University of Technology Sydney, Ultimo, 2007 NSW Australia*

[5] *Department of Mechanical/Electrical Engineering, College of Engineering, Universiti Tenaga Nasional, 43000 Kajang, Selangor, Malaysia*

[6] *Department of Agricultural Engineering, Cairo University, Giza, Egypt*

[7] *Department of Civil Engineering, University of British Columbia, Vancouver, BC V6T 1Z3, Canada*

[8] *Mechanical Engineering Department, Engineering Faculty of Diponegoro University. Jalan Prof. Soedarto SH, Tembalang, Semarang 50275, Central Java, Indonesia*

[9] *Department of Mechanical Engineering, Faculty of Engineering, International Islamic University Malaysia, 50728 Kuala Lumpur, Malaysia*

*Corresponding author: atgurvinay@gmail.com; rizwanul.buet@gmail.com

Thermogravimetric investigation and combustion performance Jatropha oil methyl ester and its blend

Thermal behavior of diesel, Jatropha methyl ester (JOME), and its B20 blend (20% of biodiesel and 80% of diesel) are examined from the profiles of Thermogravimetry - Differential Scanning calorimetry (TG-DSC) under air. TG profiles of samples indicate the mass loss steps to volatilization and combustion of methyl esters. Due to the higher temperature combustion of formed intermediate stable compounds, the peak temperature of combustion is high for JOME compared to diesel and B20 blend. DSC profiles of diesel and B20 JOME indicate an endothermic peak associated with the vaporization of methyl esters for B20 JOME and the volatilization of a small fraction of the diesel. The ignition temperature for Diesel and B20 blend is 128 °C, whereas JOME exhibits 220 °C. The burnout temperatures for the diesel, JOME, and B20 blend are 283.24 °C, 470.02 °C, and 376.92 °C, respectively. The ignition index for the B20 blend was found to be 73.73% more compared to diesel. The combustion index for the B20 blend was found to be 37.81% higher compared to diesel. B20 blend exhibits high enthalpy, better thermal stability, and a reduced peak temperature of combustion with improved combustion index and intensity of combustion nearly comparable with diesel.

Keywords: combustion; jatropha oil methyl ester; heat flow; thermal degradation.

1. Introduction

The rate at which global warming is accelerating is concerning and must be addressed. One of the fundamental reasons is the indiscriminate use of fossil fuels, which has resulted in the degradation of natural resources. Diesel engines effectively delivered efficient power while drastically harming living beings. Because these nonrenewable energy supplies are depleting, the world focuses on alternate fuel sources [1, 2]. Biofuel is a green fuel considered to be renewable [3-5]. Fuels derived from vegetable oils or

animal fat have less sulfur content, low particulate emission, and neutral contribution of CO_2 to the environment [6-9].

Stability is the major concern for using jatropha as engine fuel. Poor oxidation and thermal stability result in gum formation leading to the problem of long storage [10, 11]. Among various non-edible oil sources, jatropha oil has the potential to produce a large quantity of biodiesel [12, 13]. Double bonds in the mono-alkyl esters of biodiesels are responsible for the oxidation process, which begins with the loss of hydrogen atoms [14]. After that, newly developed radicals react with oxygen, forming peroxide, giving rise to more alkyl radicals. Furthermore, this process consumes esters and ends with the formation of stable compounds like ketones, aldehydes, etc. [5, 15, 16]. These are more harmful emissions than HC & CO. Petroleum oils are stable at distillation temperature. Straight-run gasoline (or "naphtha") is a result of fractional distillation of crude oil that boils between 30 °C and roughly 200 °C [17]. Vegetable oils contain unsaturated compounds that oxidize at room temperature to 250 °C, leading to the formation of polymeric compounds by condensation reaction [18].

Thermal analysis techniques are being used to analyze the thermal stability, oxidative reaction, volatilization, decomposition, and combustion [19-21]. One of the techniques used to evaluate thermal stability is Thermogravimetric analysis (TGA). This approach elucidates the physical (adsorption, desorption, and phase transitions) and chemical (chemisorption and thermal decomposition) phenomena of the substances being described [20]. Several researchers conducted thermal analyses to better understand the combustion behavior and stability of fossil fuels, which has a substantial impact on the industrial economy [22, 23]. Farias et al. [24] examined biodiesel blends' thermal stability in 20% passion fruit, 20% castor oil biodiesel, and 20% biodiesel blend of passion fruit and castor oil. TG curve indicates higher stability of castor oil biodiesel when compared

to that of passion fruit. The presence of oleic and linoleic acids in the passion fruit leads to low thermal stability due to high oxidation. Blends of passion fruit and castor oil biodiesel (1:1 proportions) indicate high thermal stability, whereas high stability in 1:2 proportions is due to ricinoleic acid content in castor oil. Santos et al. [25] have investigated biodiesels' thermal stability and physicochemical properties produced from cotton, sunflower, palm oil, and their B10 blends. TG-curve of the palm oil indicates a high initial temperature of decomposition and two mass loss steps, whereas one mass loss in the case of sunflower oil and cotton oil. The high onset temperature of cotton oil biodiesel indicates high thermal stability when compared to palm and sunflower oil biodiesel. Blends have a high decomposition temperature. Volli and Purkait [26] have examined the thermo-chemical behavior of mustard, soybean, olive, and Karanja oils. They have conducted TG-DTG experiments in a nitrogen atmosphere up to 600 °C with heating rates of 10, 20, 30, 50, and 100 °C/min. They have observed a single stage of decomposition. High activation energy is noticed in Karanja, followed by soybean, mustard, and olive oils. Dwivedi and Sharma [27] have studied the oxidation and thermal stability of *Pongamia* biodiesel deterioration in long storage. They have examined the oxidation stability, onset and offset temperature and activation energy on the blends of *Pongamia* biodiesel varying 100-500 ppm of pyrogallol (PY) antioxidant and 0.5 to 2 mg/L iron metal contaminants. Thermal degradation of the samples follows the first-order reaction. The addition of PY antioxidants increases the induction period and activation energy, which will be decreased with the addition of iron metal contaminants. John et al. [28] have presented the fuel properties following spectrometric methods like GC-MS, and FTIR with TG-DSC to assess the hemp (*Cannabis Sativa L.*) biodiesel quality. Results of DSC and TG-DTG are in good agreement with the GC-MS and FTIR results. Wnorowska et al. [29] have examined the effect of fuel additives on different fuels to analyze the

combustion profiles. Halloysite was used as a fuel additive and generated TG-DTG profiles for analyzing the combustion profile.

Leonardo et al. [30] authors have used thermogravimetry methods to determine the volatility parameters for diesel S10 fuel. Platinum and aluminum pans are used for experimentation from ambient temperature to 580 °C with a heating rate of 10 °C/min. Experiments were performed in both closed and open pans. When using open pans, boiling occurs at a lower temperature due to the dragging effect of purge gas. Donoso et al. [31] considered the bio waste generated from the wine industry for the oxidation stability study. Grapeseed oil fatty acid ethyl ester and methyl esters have been obtained from grape marc and bioethanol. Grapeseed oil ethyl ester satisfies the standard as per EN14214 except for oxidation stability. Natural antioxidants obtained from the extraction process were added to biofuel. Grapeseed oil fatty acid methyl ester shows improved oxidation stability compared to ethyl esters. The addition of an antioxidant improves the oxidation stability of Grapeseed oil ethyl ester, but has no effect on methyl esters.

The bulk of the publications in the literature completed engine research by testing, which is time-consuming and takes a huge quantity of fuel to forecast the combustion behavior. These experiments can be minimized through TG-DSC analysis. In the present work, thermoanalytical methods have been adopted to analyze the combustion behavior, which requires small samples. This paper examines the thermal behavior of diesel, JOME, and its B20 blend from the profiles of DSC and TG-DTG under atmospheric air. The novelty of this study is to compare diesel, *jatropha carcus,* and 20% jatropha biodiesel blend with diesel using the above-mentioned methods. Peak combustion temperature, enthalpy, onset-offset temperature, stability, ignition, and burnout temperature are reported. DTG curve is utilized and evaluated combustion index (S) and intensity of

combustion (H_f). This study will help analyze combustion behavior and storage conditions, which will be helpful in optimizing the fuel blends, thereby reducing the number of engine bench tests.

2. Materials and Testing

2.1 Materials

JOME was procured from CIDBPR (Centre for Information and Demonstration of Biofuels Production and Research), Biofuel Park Madenur, Hasan. *J. curcas* L. is a poisonous, semi-evergreen shrub or small tree, reaching a height of 6 m. The place of origin of *J. curcas* plant is Mexico. Portuguese traders spread it across Asia and Africa as a hedge plant. It belongs to the family Euphorbiaceae [32]. The blends of JOME, i.e., B20 JOME, were homogenized initially by a magnetic stirrer for 10 minutes, followed by 20 minutes in an ultrasonicator. Appropriate glassworks are used while preparing the blends by volumetric proportion (pipette, graduate beaker, and volumetric flask). **Figure 1** shows the prepared biodiesels (viz., JOME, and B20 JOME).

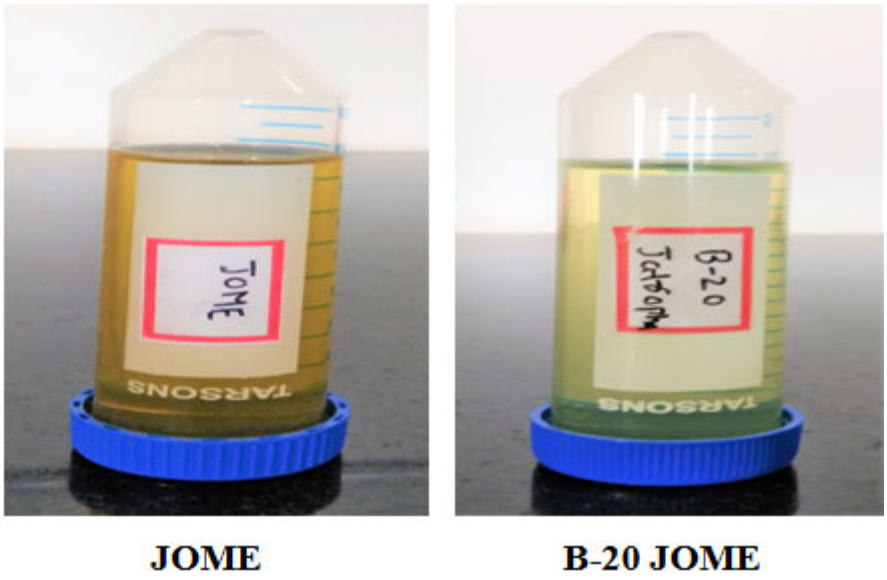

Figure 1: Biodiesel and its blends produced from *jatropha carcus*

Table 1 gives the composition of diesel, JOME, and ASTM biodiesel, whereas **Table 2** presents the properties of diesel, JOME, and its B20 blend. JOME has less carbon and hydrogen content and less calorific value when compared to that diesel due to the significant content of O_2 [33]. **Table 3** gives the fatty acid content of JOME. A high level of unsaturated fatty acids, 61.5%, reduces the fuel quality [34]. Saturated fatty acids like palmitic (16:0) and stearic (18:0) are more stable than unsaturated fatty acids like oleic (18:1) and linoleic (18:2), resulting in lower fuel quality.

Table 1: Composition (wt.%) of diesel, JOME and ASTM biodiesel

Element	Diesel	Jatropha Methyl Ester	ASTM Biodiesel
Carbon (C)	83.80	75.02	77
Hydrogen (H)	12.2	12.00	12
Nitrogen (N)	0	-	-
Sulfur (S)	0.23	-	0.05
Oxygen (O_2)	1	9.82	11
C/H ratio	7.0	6.3	-

Table 2: Properties of diesel and biodiesel

Fuel	Calorific value (MJ/kg)	Kinematic viscosity @40 °C (cSt)	Cetane value	Density (kg/m^3)	Flash point (°C)	Pour point (°C)	Cloud point (°C)
Diesel	44.22	2.87	47.8	840	76	-3	6.5
JOME	39.79	4.73	52	862.2	182.5	3	3
B20 JOME	44.10	3.99	49	840.2	93.5	-3	4

Table 3: Structure and fatty acid composition (%) of JOME

Fatty acids	Structure	Composition (%)
Lauric	12:0	-
Myristic	14:0	5
Palmitic	16:0	22
Stearic	18:0	5.5
Oleic	18:1	49.5
Linoleic	18:2	12
Linolenic	18:3	0.2
Arachidic	20:0	0.5
Others		4
Saturated		38.5
Unsaturated		61.5

2.2 Fourier transformer infrared spectroscopy (FTIR)

FTIR is used to determine the presence of different functional groups in the sample. It is also used to investigate the compounds formed by the transesterification of JOME. Interpreting infrared (IR) spectra is of immense help for structure determination. Infrared spectroscopy analysis also clarifies the concentration of bands using transmittance values. IR spectra record in the range of 3000-700 cm^{-1}. Perkin Elmer Spectrum Two FT-IR instrument made in the USA is used for the experimentation.

2.3 Thermal property analyzer

Physical properties (like density, viscosity, thermal conductivity, and specific heat) are essential for analyzing the transient phase. Experimental evaluation of these transport

properties is involved due to fuel composition variation from one to another. Because of decomposition, measurements are complex over-temperature levels. They are useful in understanding the intermolecular interaction among different biodiesel molecules and the combustion behavior. Thermal conductivity, specific heat, and thermal diffusivity are determined using Hot Disk TPS 500 Thermal Constants Analyzer made by hot disc corporation, Sweden (see **Figure 2**). TPS 500 measures the properties accurately and rapidly using two sensors, Kapton sensors (:7577*, 5465, 5501) and Teflon sensors (: 7577*, 5465, 5501). The TPS method is based on the transiently heated plane source.

Figure 2: Hot Disk TPS 500 Thermal Constants Analyzer

2.4 TG-DSC combustion experiment

DSC measures the heat flow of transition in materials in terms of temperature and time. DSC curves are obtained in a calorimetric model NETZSCH STA 449F3 made by the NETZSCH group, Germany (**Figure 3**). Atmospheric air is chosen as a medium. The heating rate is 10 °C/min. DSC consists of T-Zero calibration and Enthalpy/temperature calibration. Two experiments are performed in T-Zero calibration:(i) without a sample to obtain the baseline and (ii) with a large (95 mg) sapphire disk on both samples and

reference positions (without the pans). In enthalpy /temperature calibration, standard metal (viz., indium) was heated to its melting transition and compared heat of fusion with its theoretical value. During experimentation, the Alumina crucible pan is selected and sealed hermetically with a universal crimper, avoiding the splashing of the sample outside the pans and preventing sensor failure. Care is taken while performing experiments for liquid samples. DSC curves are analyzed in reaction intervals, peak temperature, heat flow, and enthalpy. TG analysis is performed to record mass loss in terms of increasing temperature in a controlled environment. TG-DTG curves provide the data of pure compounds or mixtures. The curves are analyzed for stability, weight loss, maximum decomposition temperature, onset, and offset temperatures.

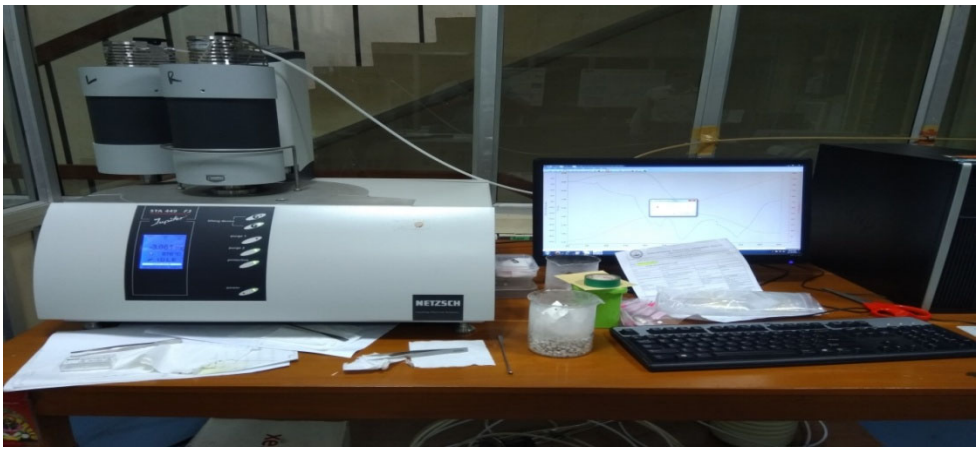

Figure 3: TG- DSC Instrument Make NETZSCH STA 449F3

2.5 Combustion characteristics of biodiesels

Combustion characteristics of diesel, JOME, and its B20 blend are evaluated in the air. Ignition temperature (T_i) is calculated as follows. Let T_{max} be the temperature at DTG_{max}. Draw tangent lines on TG-curve at the beginning of the TG curve and at T_{max}. The intersection of these tangent lines will be at the ignition temperature (T_i), as shown in stages 1 and 3 of **Figure 4**. At burnout temperature (T_b), 98% of conversion (α) occurs at

the single stage of the combustion process.

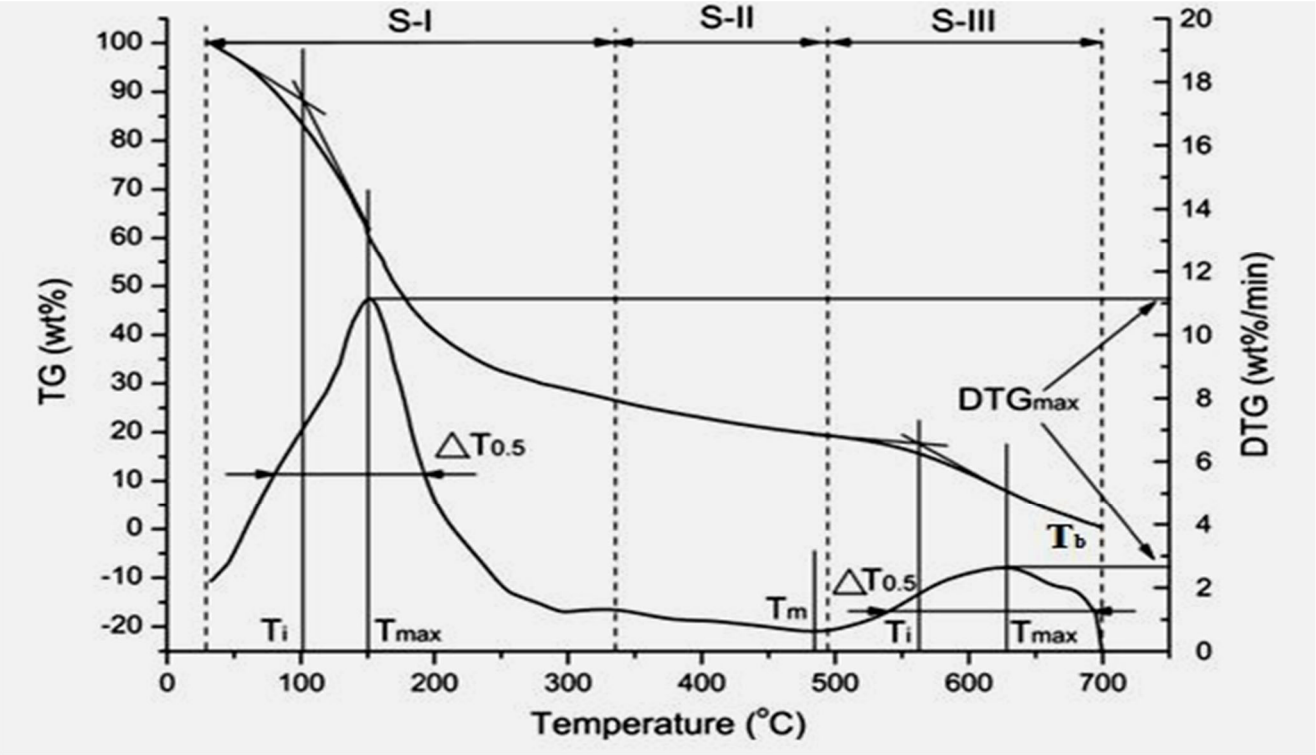

Figure 4: Combustion stages from TG-DTG curve [35]

The conversion (α) is defined as

$$\alpha_T = \frac{w_0 - w_T}{w_0 - w_f} \times 100\% \qquad (1)$$

Here, $w_0$and $w_f$are the weights at the beginning and at the end of combustion. $w_T$is the mass at temperature, *T*.

The ignition index (D_i) and the burnout index $(D_b)$are defined as

$$D_i = \frac{DTG_{\max}}{T_{\max} \times T_i} \qquad (2)$$

$$D_b = \frac{DTG_{\max}}{\Delta T_{0.5} \times T_{\max} \times T_i} \quad (3)$$

$\Delta T_{0.5}$ is the half peak width of the DTG curve

Combustion index (S) is defined as

$$S = \frac{DTG_{\max} \times DTG_{mean}}{T_b \times T_i^2} \quad (4)$$

DTG_{mean} is defined as

$$DTG_{mean} = \frac{\propto T_b - \propto T_i}{((T_b - T_i)/\beta)} \quad (5)$$

The intensity of Combustion H_f is defined as

$$H_f = T_{\max} \times \ln\left(\frac{\Delta T_{0.5}}{DTG_{\max}}\right) \times 10^{-3} \quad (6)$$

S is the parameter of combustion index and ignition and burnout characteristics high value represents the better combustion properties in equation 5. H_f is the intensity of the combustion process lesser value represents a better combustion property equation 6.

3. Result and Discussion

3.1 Fourier Transformer Infrared Spectroscopy

FTIR spectra of diesel are shown in **Figure 5**, indicating two strong bands of symmetric and asymmetric stretching vibration of C-H at 2922 cm^{-1} and 2854 cm^{-1}. The band at 1745 cm^{-1} indicates a small variation in stretching vibration due to the carbonyl group (-C=O).

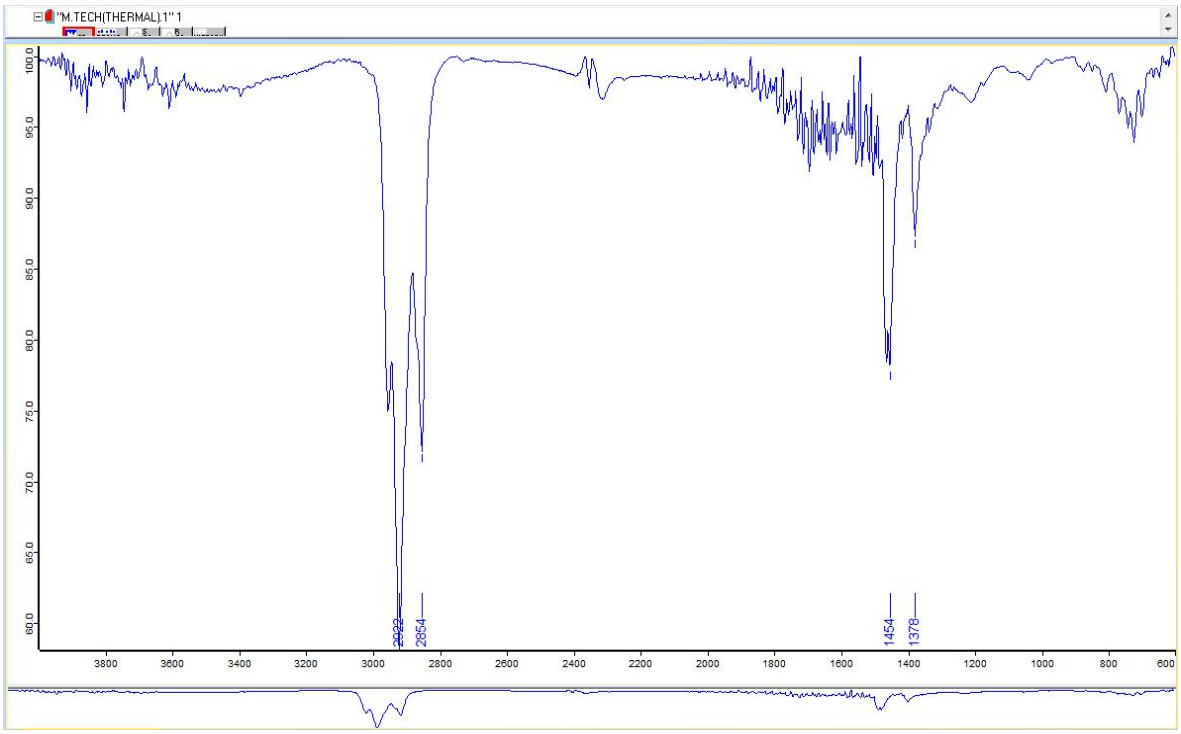

Figure 5: FTIR spectroscopy of diesel

Figure 6 shows FTIR spectra for JOME. As in diesel, the stretching vibration results in two strong bands (viz., symmetric and asymmetric stretching vibrations of C-H) at 2923 cm^{-1} and 2854 cm^{-1} [36]. The band at 1742 cm^{-1} indicates a small variation in stretching vibration due to the carbonyl group (-C=O). The bending vibration of CH_2 and CH_3 groups of biodiesel shows variations in the strong peak at 1463 cm^{-1}. Due to the wagging vibrations of the CH_2 group, the biodiesel has a strong peak at 1169 cm^{-1} [37], while the peak at 722 cm^{-1} indicates the rocking vibration of =C-H groups.

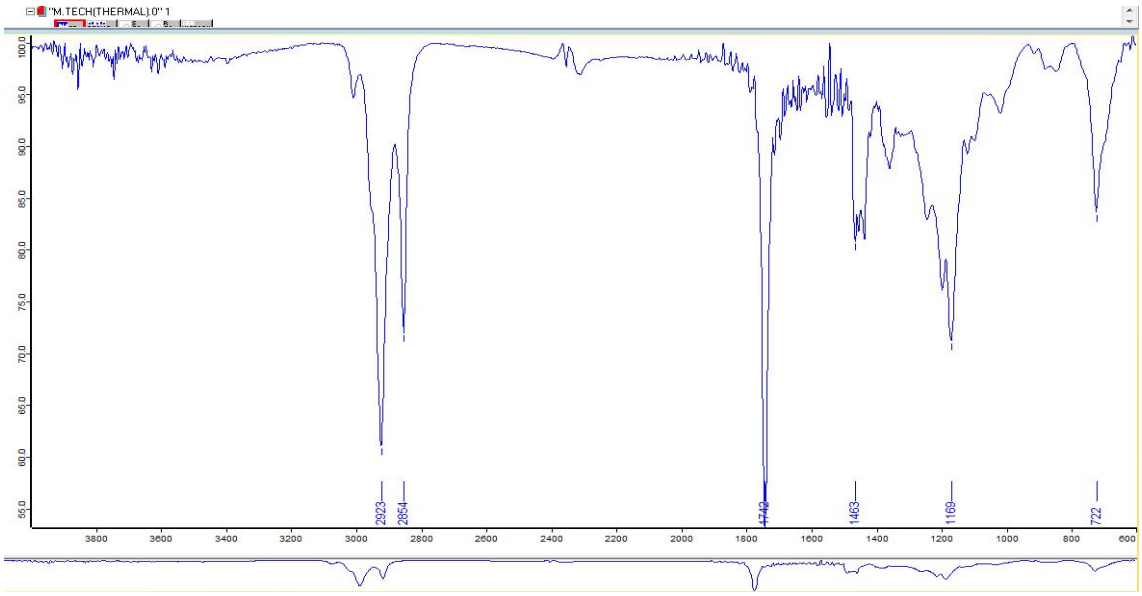

Figure 6: FTIR Spectroscopy of JOME

Figure 7 shows FTIR spectra for B20 JOME. As in diesel and JOME, the stretching vibration results in two strong bands (viz., symmetric and asymmetric stretching vibrations of C-H) at 2922 cm^{-1} and 2854 cm^{-1}. The band at 1745 cm^{-1} indicates a small variation in stretching vibration due to the carbonyl group (-C=O). The bending vibration of CH_2 and CH_3 groups of the biodiesel shows variations in strong two peaks at 1465 cm^{-1} and 1378 cm^{-1}. Due to the wagging vibrations of the CH_2 group, the biodiesel has a strong peak at 1170 cm^{-1}, while the peak at 723 cm^{-1} indicates the rocking vibration of =C-H groups.

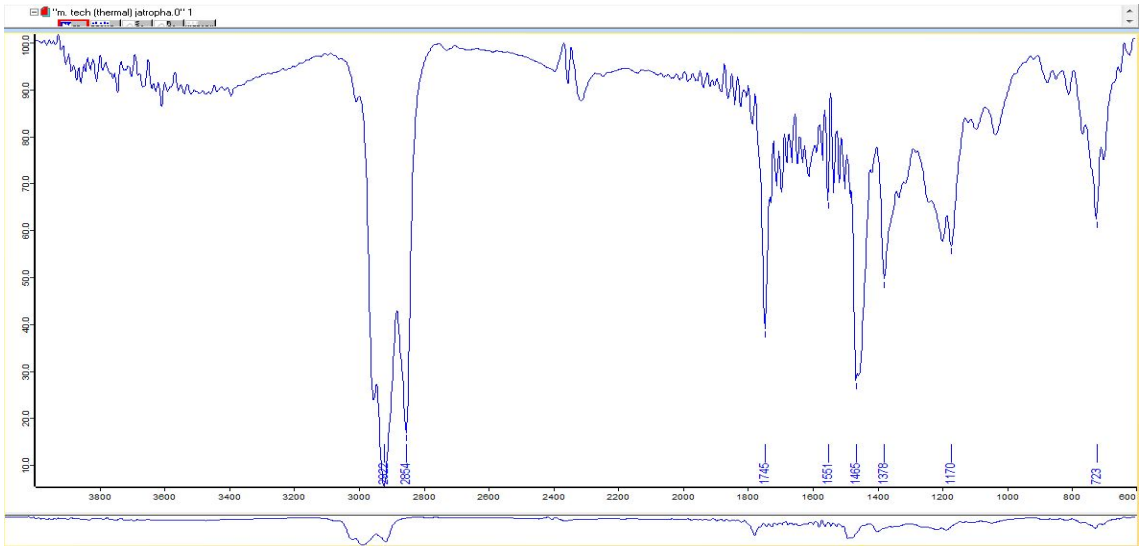

Figure 7: FTIR Spectroscopy of B20 JOME

3.2 Thermal Properties

Transport properties in **Table 4** varying the following order: Diesel >B20 JOME >JOME. Diesel possesses a high calorific value compared to JOME and B20JOME [36]. In diesel, carbon numbers range from C_5-C_{12} (i.e., low carbon number is attached to hydrogen). Decomposition of such structure becomes easy compared to FAME (fatty acid methyl esters) of biodiesel. Therefore, diesel possesses better transport properties when compared to JOME and B20 JOME.

Table 4: Thermal conductivity, thermal diffusivity and specific heat capacity

Sample	Thermal conductivity (W/mK)	Thermal diffusivity (mm^2/s)	Specific heat (MJ/m^3K)
Diesel	0.3381	1.325	0.2553
JOME	0.2358	0.4116	0.5728
B20 JOME	0.3087	0.7944	0.3886

Due to weaker double bond presence and structure possessing oxygen content, biodiesels exhibit low transport properties compared to diesel and B20 blends [38]. Diesel molecules have long-chain hydrocarbons and low ignition temperature when compared to JOME. B20JOME properties merely match with those of the diesel. This is the reason why the transport properties of the B20 blend are within the range of diesel and biodiesel. Kinematic viscosities of diesel, JOME, and B20 JOME are 2.87 cSt, 4.73 cSt, and 3.99 cSt, respectively. The diesel, JOME, and B20 JOME densities are 840 kg/m^3, 862.2 kg/m^3, and 840.2 kg/m^3, respectively. Both viscosity and density decrease with increasing temperature, leading to buoyancy force. It will be opposed by the viscous force for the heat flow. Transport properties decrease with increasing the content in biodiesel [39, 40]. B20 JOME will be an alternative to diesel.

3.3 DSC analysis

Generally, the combustion of hydrocarbons exhibits an exothermic reaction. DSC thermogram of diesel (**Figure 8**) indicates an endothermic reaction at 34-100 °C. This is termed an evaporation zone where fuel prepares for combustion a small fraction of diesel volatile up occurring only one step endothermic cracking reaction. It is termed diesel distillation [41, 42]. Combustion peak temperature occurs at 250.4 °C with enthalpy 130.4 J/g as diesel consists of C_5-C_{12} with a boiling range of 180-371 °C. Further, it starts burning and dissipating more energy to the environment.

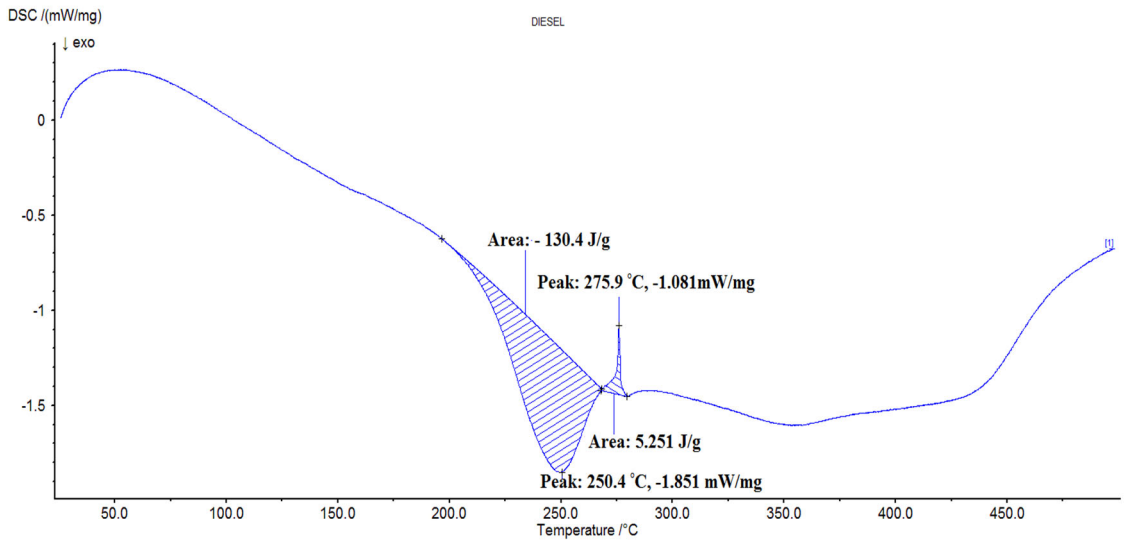

Figure 8: DSC combustion curve for diesel

DSC combustion curve of JOME (**Figure 9**) exhibits a reaction zone occurring at 43-435°Cwith a peak at 292.1°C. The combustion reaction zone of biodiesel occurs at a high-temperature range when compared to diesel—direct use of biodiesel results in hard burning in engine motors. A high cetane number of fuels in engines experience a short delay in biodiesel burning [9]. Low Cetane number biodiesels lead time a delay in burning, resulting in insufficient engine performance [43, 44]. Biodiesel has a faster combustion behavior and a higher combustion temperature than conventional diesel due to its higher oxygen content. A higher cetane number in JOME yields a short delay time in fuel combustion, and more time is taken for complete combustion. JOME combustion reaction range, as well as combustion peak temperature, can be expected more when compared to those of diesel [38]. The combustion phenomenon of JOME exhibits an exothermic reaction in the air due to a weaker double bond presence [45, 46].

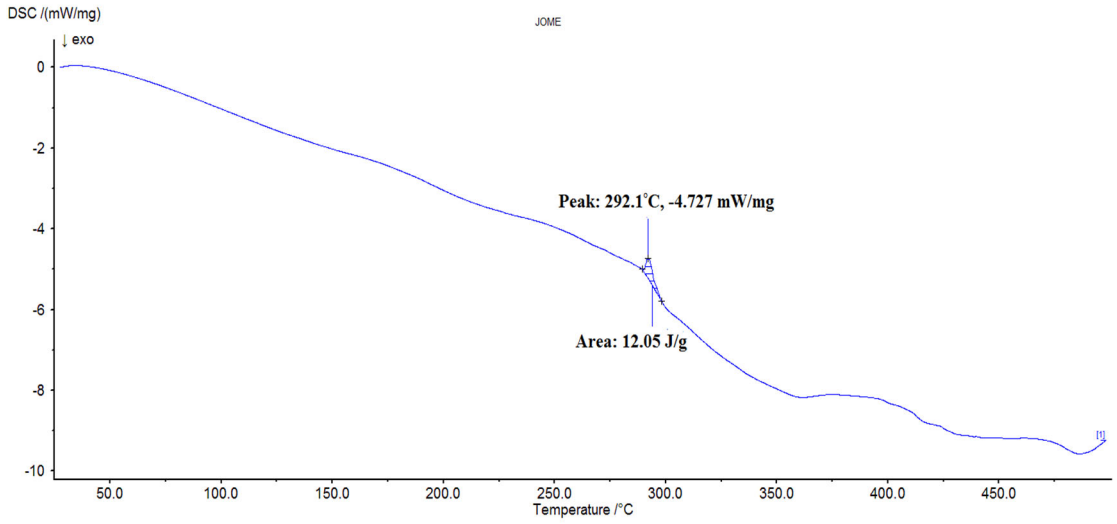

Figure 9: DSC combustion curve for JOME

The combustion thermogram of the B20 blend (**Figure 10**) is very close to diesel, with a reaction zone occurring at 63-465°C. Initially, it shows an endothermic reaction up to 63°C. The peak temperature of combustion in **Table 5** is 266.5 °C, close to diesel, with an enthalpy of 147.5 J/g. In the first reaction, interval combustion of diesel takes place, whereas, in the second reaction, interval biodiesel combustion takes place [47]. Biodiesel and diesel molecules perform a homogenous mixture. Hence, B20 combustion is close to diesel, and the reaction starts early, resulting in easy combustion. From there action region of the DSC combustion curve [48, 49], the cetane number of biodiesel is found to be less

when compared to that of diesel. Blending is necessary. Otherwise, direct use of biodiesel in the engine results in time delay leading to insufficient engine performance. **Table 5** gives the comparison of the reaction region, the peak temperature of combustion, heat flow, and enthalpy.

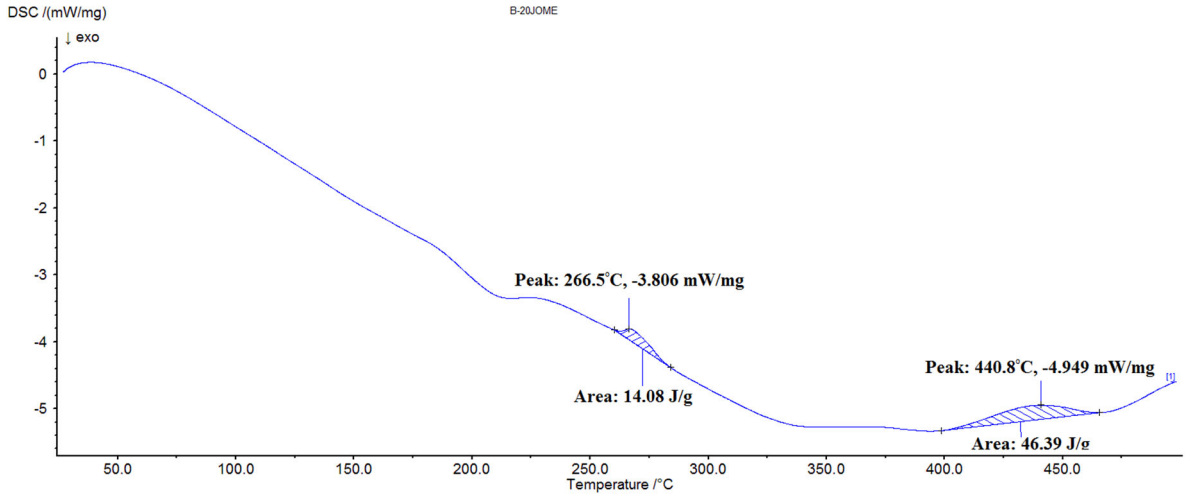

Figure 10: DSC combustion curve for B20 JOME

Table 5: Heat flow and enthalpy at peak temperature

Sample	Reaction Region (°C)	Peak Temperature (°C)	Heat flow (mW/mg)	Enthalpy (J/g)
Diesel	34-270	250.4	-1.851	130.4
JOME	43-435	292.1	-4.727	12.05
B20 JOME	63-465	266.5	-3.808	147.5

3.4 Thermal Stability Analysis

TG-DTG curve of diesel in synthetic air presents one complex mass loss step at 40-280°C. Behavior and properties depend on the length of diesel molecules [50]. Longer chains of molecules have higher boiling points. The opposite properties of gasoline characterize

diesel. Hydrocarbon molecules must oxidize with the formation of peroxides initially. Other products of incomplete oxidation are for auto-ignition to start easily [51]. Initially, there is evaporation and combustion of methyl esters, as well as the evaporation and combustion of the other components of diesel-like naphthenes, paraffin, olefins, and aromatics with a C_{12}-C_{18}.

In the TGA-DTG curve of diesel in **Figure 11**, combustion reaction occurs between 40-495.74 °C with a peak temperature of 184.5 °C. Diesel fuel mainly contains C_5 –C_{12} with a boiling range of 180- 376 °C; at around 45 °C, diesel starts to burn and dissipate energy to the environment at 99.50% of mass loss occurs at 498.1 °C with 47.49 min of time span, remaining 0.5% mass loss represents soot particle which is not burned out [52].

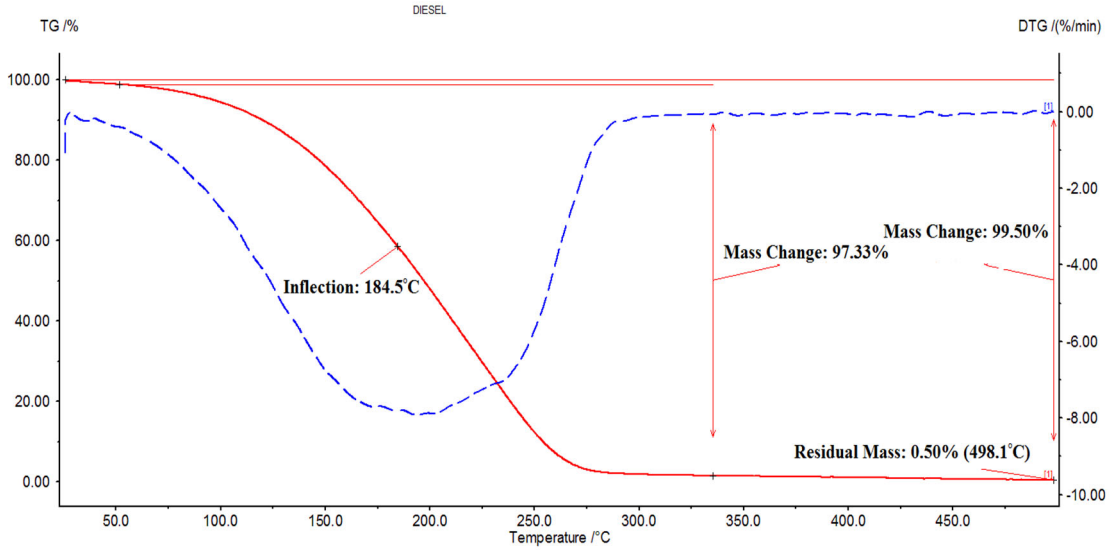

Figure 11: TG-DTG curve for Diesel

JOME exhibits the reaction at 140-490 °C with a peak temperature of 277.3 °C (**Figure 12**). Biodiesel shows two steps of the reaction. According to literature, JOME has major percentage fatty acid content of oleic acid, palmitic acid, linolenic acid, and stearic acid are 49.5%, 22%, 12%, and 5.5%, respectively. The transesterification reaction mechanism makes the biodiesel less stable. Also, the monoglycerides molecules make the sample less stable [53]. Initially, there is the evaporation of methyl esters followed by the decomposition of mono, di, and triglycerides and fatty acids with high carbon oleic and linoleic [40, 54]. The carbonization of the sample is with 1.64%weight loss. The total

loss is ≈98.36%. The combustion process takes place for a time span of 47.43 min. B20 JOME exhibits only one reaction interval, indicating better diesel and biodiesel mixing.

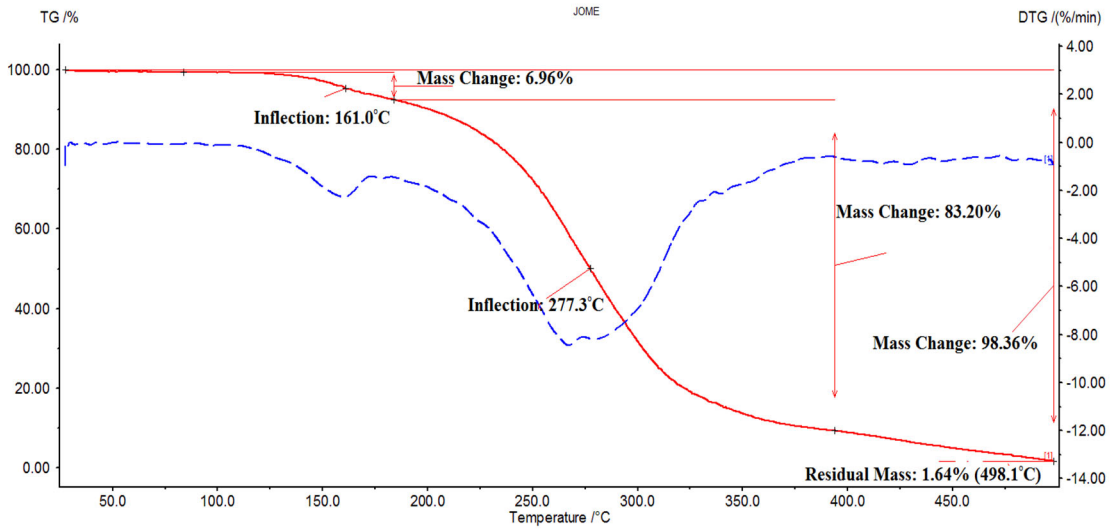

Figure 12: TG-DTG curve for JOME

Figure 13 shows the TG-DTG curve for B20 JOME. TG-DTG thermogram of diesel and B20 blend are very close to each other, and weight losses are lower than pure biodiesel [55, 56]. The blend starts to decompose from 40°C to 430°Cwith a peak temperature of 182.8 °C. Combustion of B20 blend takes place for the time span of 47.39 min with residual mass loss of 0.73%. The first reaction is the evaporation of the methyl esters and the light fraction of carbons [57, 58]. The second reaction is the decomposition of the mono, di, and triglycerides and methyl esters of fatty acids with high carbon content [59, 60]. Finally, the carbonization of the sample is from 400 to 500 °C with a mass loss of 99.27%.

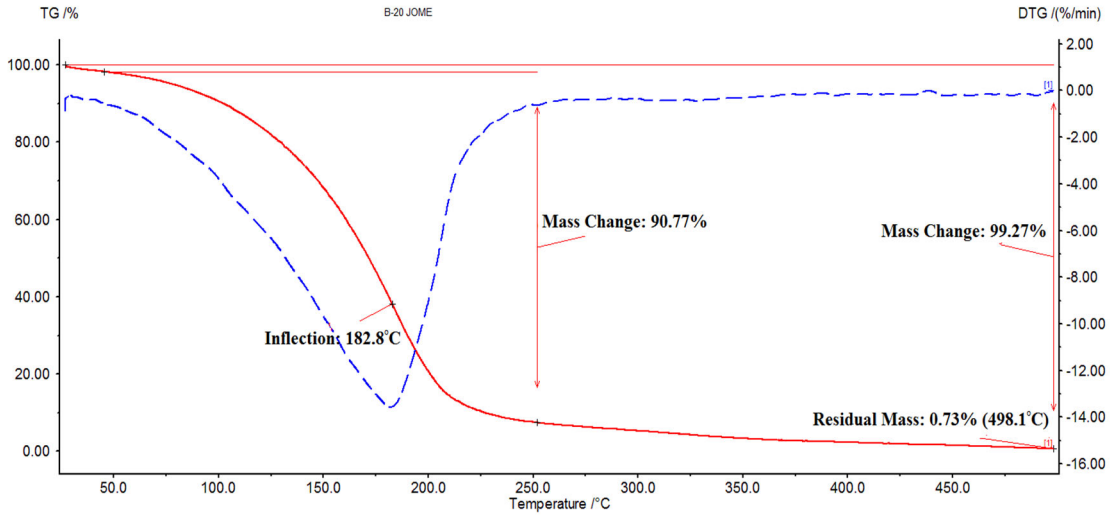

Figure 13: TG-DTG curve for B20 JOME

Diesel is less thermally stable when compared to biodiesel due to greater tension in chains of the complex structured biodiesel [56]. Hence, the thermal stability of the blends decreases with increasing the proportion of the blend. The high viscosity of the biodiesel leads slow evaporation process and high thermal stability of fuels [61]. It is observed that initially, the TG curves attain ascent because of buoyancy and molecular adsorption effect, while TGA curves are in descending trend with increasing temperature due to volatilization of weak chemical bonds and small molecules of biodiesel blends [25, 62]. A single well-defined mass loss step could be clearly observed for all TG curves, which describes the volatilization and decomposition. The decomposition temperature increases with increasing the proportion of biodiesel in blends. **Table 6** gives the comparison of onset, offset, reaction region, maximum temperature and weight loss. JOME presents low onset temperature and high volatility. It approaches the diesel characteristics and improves the fuel properties.

Table 6: On-set, offset, reaction region, maximum temperature, and weight loss biodiesels

Sample	On-set temperature T_e (°C)	Off-set temperature T_o (°C)	Reaction Region (°C)	Decomposition Temperature, T_{max} (°C)	Weight loss (%) at 498.1°C

Diesel.	140	265	40-280	184.5	99.50
JOME	146	334	140-490	277.3	98.36
B20 JOME	130	230	40-430	182.8	99.27

Table 7 presents ignition temperature, burnout temperature, and maximum DTG. Compared to JOME, diesel and B20 blends have less devolatilization stage, and JOME degradation represents three stages of the process as in Ren et al. [35]. **Table 8** presents the combustion index, which differs in air and oxidation environments due to combustion's high degradation temperature [63]. Low mass degradation in the later stage is due to a low combustion index. JOME has significant mass degradation after the third stage, leading to high combustion and hard burning intensity.

Table 7: Ignition, burnout temperature, DTG_{max} and T_{max} of Diesel, JOME, and B20 JOME.

Sample	**Ignition Temperature (°C)**	**Burnout Temperature (°C)**	**DTG max**	**Tmaxcorres DTG max(°C)**
DIESEL	128	283.24	7.92	184.5
JOME	220	470.02	8.44	267.52
B20 JOME	128	376.96	13.56	181.965

Table 8: Combustion characteristics of Diesel, JOME, and B20 JOME.

Sample	**Ignition Index D_i x 10^{-4}**	**Burnout index D_b x 10^{-6}**	**Combustion index parameter Sx10^{-6} (wt% min^{-2} $°C^{-3}$)**	**Intensity of Combustion**

	(wt.% min^{-1} °C^{-2})	(wt.% min^{-1} °C^{-3})		
DIESEL	3.35	3.35	41.6	0.467
JOME	1.43	6.87	77.74	0.591
B20 JOME	5.82	4.6	57.33	0.318

4. Conclusion

DSC and TG-DTG are useful tools for assessing biodiesel's combustion behavior and thermal stability and its blend. Thermogravimetry and calorimetric profiles of the samples indicate the relation of mass loss steps to volatilization and combustion methyl esters. On the basis of TG curves, thermal stability is established as JOME>B20 JOME>Diesel. Diesel and B20 JOME degradation start from 40 °C, whereas JOME degradation starts from 140°C. JOME is thermally stable up to 140 °C. This matches well with the onset and offsets temperatures. JOME presents lower onset temperature and high volatility. It approaches the diesel characteristics and improves the fuel properties. JOME presents more decomposition steps with high decomposition temperatures indicative of the formation of a more stable compound due to the oxidation process. The combustion of formed stable compounds takes place at high temperatures. The peak temperature of combustion for diesel, JOME, and B20 JOME are 250.4 °C, 292.1 °C, and 266.5°C, respectively. DSC profiles of the diesel and B20 JOME show an endothermic peak related to the vaporization of methyl esters for B20 JOME and the volatilization of a small fraction of the diesel. Biodiesel exhibits high enthalpy despite satisfactory performance as a fuel, its high viscosity causing poor fuel atomization in the combustion of the engine and serious engine problems requiring blending with petroleum diesel. B20 blend exhibits high enthalpy when compared to a diesel with reduced peak temperature.

Acknowledgment

The authors would like to express their gratitude to the Visvesvarayya Technological University, Belgaum, and the Sophisticated Analytic instrumentation facility center,

Indian Institute of Technology, Madras, for providing facilities to carry out experiments.

Funding

This work is supported by the Universiti Tenaga Nasional grant no. IC6-BOLDREFRESH2025 (HCR) under the BOLD2025 Program.

Data Availability Statement

The data supporting this study's findings are available from the corresponding author upon reasonable request.

Competing interests

The authors declare that they have no competing interests.

References

[1] Kumar S, Dinesha P. Use of alternative fuels in compression ignition engines: a review. Biofuels. 2019;10(4):525-35.
[2] Mishra VK, Goswami R. A review of production, properties and advantages of biodiesel. Biofuels. 2018;9(2):273-89.
[3] Thiyagarajan S, Varuvel E, Karthickeyan V, Sonthalia A, Kumar G, Saravanan CG, et al. Effect of hydrogen on compression-ignition (CI) engine fueled with vegetable oil/biodiesel from various feedstocks: A review. International Journal of Hydrogen Energy. 2022.
[4] Fattah IMR, Ong HC, Mahlia TMI, Mofijur M, Silitonga AS, Rahman SMA, et al. State of the Art of Catalysts for Biodiesel Production. Frontiers in Energy Research. 2020;8(101).
[5] Viswanathan K, Ikhsan Taipabu M, Wu W. Novel Petit grain bitter orange waste peel oil biofuel investigation in diesel engine with modified fuel injection pressure and bowl geometry. Fuel. 2022;319:123660.
[6] Seela CR, Ravi Sankar B, Sai Kiran D. Influence of biodiesel and its blends on CI engine performance and emissions: a review. Biofuels. 2017;8(1):163-79.
[7] Kumar A, Subramanian KA. Experimental investigation on effects of karanja biodiesel (B100) on performance, combustion, and regulated and GHG emissions characteristics of an automotive diesel engine. Biofuels. 2020;11(3):239-50.
[8] Swaminathan C, Sarangan J, Michael BS. Investigation of performance and emission characteristics of IC engine using sunflower oil methyl ester as fuel with oxygenated additive and EGR. Biofuels. 2019;10(5):583-9.

[9] Veza I, Afzal A, Mujtaba MA, Tuan Hoang A, Balasubramanian D, Sekar M, et al. Review of artificial neural networks for gasoline, diesel and homogeneous charge compression ignition engine. Alexandria Engineering Journal. 2022;61(11):8363-91.
[10] Manaf ISA, Embong NH, Khazaai SNM, Rahim MHA, Yusoff MM, Lee KT, et al. A review for key challenges of the development of biodiesel industry. Energy Conversion and Management. 2019;185:508-17.
[11] Iyer R. A review on the role of allylic and bis allylic positions in biodiesel fuel stability from reported lipid sources. Biofuels (London). 2017;8(5):543-54.
[12] Kavitha KR, Beemkumar N, Rajasekar R. Experimental investigation of diesel engine performance fuelled with the blends of Jatropha curcas, ethanol, and diesel. Environmental Science and Pollution Research. 2019;26(9):8633-9.
[13] Borah N, Mapelli S, Pecchia P, Mudoi KD, Chaliha B, Gogoi A, et al. Variability of growth and oil characteristics of Jatropha curcas L. in North-east India. Biofuels. 2021;12(3):327-37.
[14] Azad AK, Adhikari J, Halder P, Rasul MG, Hassan NMS, Khan MMK, et al. Performance, Emission and Combustion Characteristics of a Diesel Engine Powered by Macadamia and Grapeseed Biodiesels. Energies. 2020;13(11):2748.
[15] Viswanathan K, Wang S, Esakkimuthu S. Impact of yttria stabilized zirconia coating on diesel engine performance and emission characteristics fuelled by lemon grass oil biofuel. Journal of Thermal Analysis and Calorimetry. 2021;146(5):2303-15.
[16] Taipabu MI, Viswanathan K, Wu W, Nagy ZK. Production of renewable fuels and chemicals from fats, oils, and grease (FOG) using homogeneous and heterogeneous catalysts: Design, validation, and optimization. Chemical Engineering Journal. 2021;424:130199.
[17] Thomas A. Chapter Five - Automotive fuels. In: Arcoumanis C, editor. Internal Combustion Engines: Academic Press; 1988. p. 213-70.
[18] Xia Y, Larock RC. Vegetable oil-based polymeric materials: synthesis, properties, and applications. Green Chemistry. 2010;12(11):1893-909.
[19] Rial RC, de Freitas ON, Santos Gd, Nazário CED, Viana LH. Evaluation of the oxidative and thermal stability of soybean methyl biodiesel with additions of dichloromethane extract ginger (Zingiber officinale Roscoe). Renewable Energy. 2019;143:295-300.
[20] Balajii M, Niju S. Biochar-derived heterogeneous catalysts for biodiesel production. Environmental Chemistry Letters. 2019;17(4):1447-69.
[21] Lamprecht I. Chapter 4 - Combustion Calorimetry. In: Kemp RB, editor. Handbook of Thermal Analysis and Calorimetry: Elsevier Science B.V.; 1999. p. 175-218.
[22] Chauhan BS, Kumar N, Cho HM. A study on the performance and emission of a diesel engine fueled with Jatropha biodiesel oil and its blends. Energy. 2012;37(1):616-22.
[23] Banapurmath NR, Tewari PG, Hosmath RS. Performance and emission characteristics of a DI compression ignition engine operated on Honge, Jatropha and sesame oil methyl esters. Renewable Energy. 2008;33(9):1982-8.
[24] Farias RMC, Conceição MM, Candeia RA, Silva MCD, Fernandes VJ, Souza AG. Evaluation of the thermal stability of biodiesel blends of castor oil and passion fruit. Journal of Thermal Analysis and Calorimetry. 2011;106(3):651-5.
[25] Santos AGD, Caldeira VPS, Souza LD, Oliveira DS, Araujo AS, Luz GE. Study of the thermal stability by thermogravimetry for oil, biodiesel and blend (B10) of different oilseeds. Journal of Thermal Analysis and Calorimetry. 2016;123(3):2021-8.
[26] Volli V, Purkait MK. Physico-chemical properties and thermal degradation studies of commercial oils in nitrogen atmosphere. Fuel. 2014;117:1010-9.

[27] Dwivedi G, Sharma MP. Experimental investigation on thermal stability of Pongamia Biodiesel by thermogravimetric analysis. Egyptian Journal of Petroleum. 2016;25(1):33-8.
[28] John CB, Solamalai AR, Jambulingam R, Balakrishnan D. Estimation of fuel properties and characterization of hemp biodiesel using spectrometric techniques. Energy Sources, Part A: Recovery, Utilization, and Environmental Effects. 2020:1-18.
[29] Wnorowska J, Ciukaj S, Kalisz S. Thermogravimetric Analysis of Solid Biofuels with Additive under Air Atmosphere. Energies. 2021;14(8):2257.
[30] Leonardo RS, Murta Valle ML, Dweck J. Thermovolumetric and thermogravimetric analysis of diesel S10. Journal of Thermal Analysis and Calorimetry. 2020;139(2):1507-14.
[31] Donoso D, Bolonio D, Lapuerta M, Canoira L. Oxidation Stability: The Bottleneck for the Development of a Fully Renewable Biofuel from Wine Industry Waste. ACS Omega. 2020;5(27):16645-53.
[32] Fattah IMR, Masjuki HH, Kalam MA, Wakil MA, Rashedul HK, Abedin MJ. Performance and emission characteristics of a CI engine fueled with Cocos nucifera and Jatropha curcas B20 blends accompanying antioxidants. Industrial Crops and Products. 2014;57:132-40.
[33] Singh D, Sharma D, Soni SL, Inda CS, Sharma S, Sharma PK, et al. A comprehensive review of physicochemical properties, production process, performance and emissions characteristics of 2nd generation biodiesel feedstock: Jatropha curcas. Fuel. 2021;285:119110.
[34] Swathi D, Gopa BV, Rao PV, Raju GMJ. Optimization of Jatropha Methyl Ester and Study of its Physico-Chemical Properties using GC-MS and FT-IR Analysis. Austin Chemical Engineering. 2016;3(2):1027.
[35] Ren X, Meng J, Moore AM, Chang J, Gou J, Park S. Thermogravimetric investigation on the degradation properties and combustion performance of bio-oils. Bioresource Technology. 2014;152:267-74.
[36] Posom J, Sirisomboon P. Evaluation of the thermal properties of Jatropha curcas L. kernels using near-infrared spectroscopy. Biosystems engineering. 2014;125:45-53.
[37] El-Seesy AI, Xuan T, He Z, Hassan H. Enhancement the combustion aspects of a CI engine working with Jatropha biodiesel/decanol/propanol ternary combinations. Energy Conversion and Management. 2020;226:113524.
[38] Atgur V, Manavendra G, Desai GP, Nageswara Rao B. Thermogravitometry and calorimetric evaluation of honge oil methyl ester and its B-20 blend. Cleaner Engineering and Technology. 2022;6:100367.
[39] Giuliano Albo PA, Lago S, Wolf H, Pagel R, Glen N, Clerck M, et al. Density, viscosity and specific heat capacity of diesel blends with rapeseed and soybean oil methyl ester. Biomass and Bioenergy. 2017;96:87-95.
[40] Freire LMS, Bicudo TC, Rosenhaim R, Sinfrônio FSM, Botelho JR, Carvalho Filho JR, et al. Thermal investigation of oil and biodiesel from Jatropha curcas L. Journal of Thermal Analysis and Calorimetry. 2009;96(3):1029-33.
[41] Abdullah BM, Yusop RM, Salimon J, Yousif E, Salih N. Physical and Chemical Properties Analysis of Jatropha curcas Seed Oil for Industrial Applications. International Journal of Chemical Science and Engineering. 2013;7(12):183-6.
[42] Vossoughi S, El-Shoubary YM. Kinetics of liquid hydrocarbon combustion using the DSC technique. Thermochimica Acta. 1990;157(1):37-44.
[43] Xue J, Grift TE, Hansen AC. Effect of biodiesel on engine performances and emissions. Renewable and Sustainable Energy Reviews. 2011;15(2):1098-116.

[44] Teoh YH, Masjuki HH, Kalam MA, Amalina MA, How HG. Effects of Jatropha biodiesel on the performance, emissions, and combustion of a converted common-rail diesel engine. RSC Advances. 2014;4(92):50739-51.
[45] Garcia-Perez M, Adams TT, Goodrum JW, Das KC, Geller DP. DSC studies to evaluate the impact of bio-oil on cold flow properties and oxidation stability of bio-diesel. Bioresource Technology. 2010;101(15):6219-24.
[46] Atgur V, Manavendra G, Desai GP, Nageswara Rao B. Thermal characterisation of dairy washed scum methyl ester and its b-20 blend for combustion applications. International Journal of Ambient Energy. 2021:1-11.
[47] Dunn RO. Thermal analysis of alternative diesel fuels from vegetable oils. Journal of the American Oil Chemists' Society. 1999;76(1):109-15.
[48] Mohammed MN, Atabani AE, Uguz G, Lay C-H, Kumar G, Al-Samaraae RR. Characterization of Hemp (Cannabis sativa L.) Biodiesel Blends with Euro Diesel, Butanol and Diethyl Ether Using FT-IR, UV–Vis, TGA and DSC Techniques. Waste and Biomass Valorization. 2020;11(3):1097-113.
[49] Peer MS, Kasimani R, Rajamohan S, Ramakrishnan P. Experimental evaluation on oxidation stability of biodiesel/diesel blends with alcohol addition by rancimat instrument and FTIR spectroscopy. Journal of Mechanical Science and Technology. 2017;31(1):455-63.
[50] Silva WC, Castro MPP, Perez VH, Machado FA, Mota L, Sthel MS. Thermal degradation of ethanolic biodiesel: Physicochemical and thermal properties evaluation. Energy. 2016;114:1093-9.
[51] Misutsu MY, Cavalheiro LF, Ricci TG, Viana LH, de Oliveira SC, Junior AM, et al. Thermoanalytical Methods in Verifying the Quality of Biodiesel. In: Biernat K, editor. Biofuels - Status and Perspective: IntechOpen; 2015.
[52] de Oliveira TF, Dweck J. Liquid phase oxidation quantitative analysis of biodiesel/diesel blends by differential TG and DTA. Journal of Thermal Analysis and Calorimetry. 2018;134(3):1953-63.
[53] Almazrouei M, Janajreh I. Thermogravimetric study of the combustion characteristics of biodiesel and petroleum diesel. Journal of Thermal Analysis and Calorimetry. 2019;136(2):925-35.
[54] Damasceno SS, Rosenhaim R, Gondim AD, Tavares MLA, Queiroz N, Santos IMG, et al. Flow properties of biodiesel: correlation between TMDSC and dynamic viscosity. Journal of Thermal Analysis and Calorimetry. 2013;114(3):1239-43.
[55] Nicolau CL, Klein ANV, Silva CAA, Fiorucci AR, Stropa JM, Santos EO, et al. Thermal Properties of the Blends of Methyl and Ethyl Esters Prepared from Babassu and Soybean Oils. Journal of the Brazilian Chemical Society. 2018;29(8):1672–9.
[56] Candeia RA, Freitas JCO, Souza MAF, Conceição MM, Santos IMG, Soledade LEB, et al. Thermaland rheological behavior of diesel and methanol biodiesel blends. Journal of Thermal Analysis and Calorimetry. 2007;87(3):653-6.
[57] Dantas MB, Albuquerque AR, Soledade LEB, Queiroz N, Maia AS, Santos IMG, et al. Biodiesel from soybean oil, castor oil and their blends. Journal of Thermal Analysis and Calorimetry. 2011;106(2):607-11.
[58] Mujtaba MA, Muk Cho H, Masjuki HH, Kalam MA, Ong HC, Gul M, et al. Critical review on sesame seed oil and its methyl ester on cold flow and oxidation stability. Energy Reports. 2020;6:40-54.
[59] Conceição MM, Fernandes VJ, Araújo AS, Farias MF, Santos IMG, Souza AG. Thermal and Oxidative Degradation of Castor Oil Biodiesel. Energy & Fuels. 2007;21(3):1522-7.

[60] Zhao H, Cao Y, Orndorff W, Cheng Y-H, Pan W-p. Thermal behaviors of soy biodiesel. Journal of Thermal Analysis and Calorimetry. 2012;109(3):1145-50.
[61] Shancita I, Masjuki HH, Kalam MA, Reham SS, Shahir SA. Comparative Analysis on Property Improvement Using Fourier Transform Infrared Spectroscopy (FT-IR) and Nuclear Magnetic Resonance (NMR) (1H and 13C) Spectra of Various Biodiesel Blended Fuels. Energy & Fuels. 2016;30(6):4790-805.
[62] Jain S, Sharma MP. Correlation development between the oxidation and thermal stability of biodiesel. Fuel. 2012;102:354-8.
[63] Niu S-l, Han K-h, Lu C-m. Characteristic of coal combustion in oxygen/carbon dioxide atmosphere and nitric oxide release during this process. Energy Conversion and Management. 2011;52(1):532-7.